WIS-98/23/Sept.-DPP

First Measurements of Ionization Clusters on the DNA Scale in a Wall-less Sensitive Volume

S. Shchemelinin, A. Breskin, R. Chechik
Department of Particle Physics, the Weizmann Institute of Science, Rehovot 76100, Israel

P. Colautti
INFN Laboratori Nazionali di Legnaro, Via Romea, 4, I-35020 Legnaro, Italy

R. W. M. Schulte
Department of Radiation Medicine, Loma Linda University Medical Center, Loma Linda, CA 92354, USA

Abstract

A nanodosimetric technique and first ionization cluster spectra on the DNA scale are presented. Single radiation-induced ions are extracted through a small aperture from a wall-less sensitive volume formed in a tissue-equivalent gas; after acceleration in vacuum, the ions are counted by an electron multiplier. Low ion diffusion permits forming well defined tissue-equivalent sensitive volumes, down to the scale of 0.1 *nm*; the upper limit is of the order of a few tens of *nm*. Distributions of ionization clusters deposited by α-particles in sensitive volumes down to $1.1nm \times 1\ nm$ (diameter×length) are presented, with the relevance to nanodosimetric studies on the DNA scale. Present limitations and possible improvements are discussed.

Radiation Protection Dosimetry, in press

1 Introduction

A nanodosimetric technique and first ionization cluster spectra in small dilute gas volumes, simulating the DNA sizes, are presented in this article.

According to contemporary radiobiological concepts, the failure to repair radiation induced DNA damage can lead to cell death or mutation. More recently it has been hypothesized that radiation energy deposits directly within the DNA helix or in the surrounding layers of water molecules may lead to a local concentration of individual DNA lesions such as base damages and strand breaks[1]. The initiating events for these so-called multiply damaged sites are local clusters of ionization, which have been predicted by theoretical track structure calculations based on Monte Carlo codes[2]. Multiply damaged sites are assumed to present a problem for the cellular repair system and are likely to represent biologically relevant DNA damage[3]. The measurement of local ionization clusters in DNA-size volumes demands investigation and development of novel nanodosimetric devices, as these would be most relevant to assess DNA and chromatin damage[4]. As the interest shifts from micrometer dimensions, e.g., the diameter of a cell nucleus ($\sim$ 10 μm) or the interaction range between chromosome breaks ($\sim$ 1 μm), to nanometer dimensions, e.g., the diameter of chromatin fibres ($\sim$ 25 nm) or DNA helix ($\sim$ 2 nm)[5], the volumes in which ionizations are measured should also be in the range of 1-30 nm accross. The results of experimental nanodosimetric studies, combined with those of direct radiobiological investigations, could provide a better understanding of the mechanism of radiation damage to living cells and the reason why some damaged DNA escapes repair and results in cancer or cell death. They would also provide valuable input for biophysical models of cellular radiation damage[6]. There is a variety of practical applications in radiation protection and monitoring, as well as in radiotherapy.

Ordinary microdosimetry deals with ionization distributions in tissue-equivalent spherical gas volumes of 0.2 - 10 μm in diameter, i.e. at the level of the nuclei and chromosomes. Tissue-equivalent proportional counters (TEPC) are generally used. The counter integrates the charge deposited in a single event, yielding, after gas multiplication, a pulse proportional to the deposited energy.

There have been many attempts to minimize the tissue-equivalent sensitive volume size in TEPCs[7, 8, 9]; the smallest achieved cavity size in an ultraminiature counter corresponds to 5 nm[8]. However, the interaction of the ionizing particles with the cavity walls distorts the measurements, which is particularly problematic for cavity sizes below the track radius. A different method[10, 11, 12], which is based on a drift chamber coupled to a single-electron counter, should permit formation of wall-less sensitive volumes. This electron counting technique measures the number of ionizations by counting pulses induced by individual ionization electrons. The ionization volume is coupled to a gas electron multiplier by a small aperture which determines the dimensions of the sensitive volume. Compared to proportional counters, the single electron counting technique provides a measure of the deposited energy with an improved resolution; it is independent of avalanche fluctuations, because it measures in a direct way each individual ionization electron. This method, intensively investigated by us, is, however, diffusion-limited, down to a size of a wall-less sensitive volume of the order of ten tissue-equivalent nanometers. This limitation originates form the fact, that under conditions corresponding to small tissue-equivalent lengths, the ionization electrons undergo

a quasi-ballistic transport, with diffusion that strongly depends on their initial energy.

Another recent nanodosimetric approach[13], also relying on the registration of deposited electrons, consists in optically imaging the fine structure of ionizing particle tracks traversing a low-pressure gas volume. The ionization electrons along the track induce avalanches, of which the emitted light is recorded with an intensified CCD camera. The technique should permit recording of radiation-induced ionization patterns in a few micrometer size tissue-equivalent sensitive volume, with a resolution in the range a few tens of nanometers. The total deposited energy is derived from the charge integrated by the CCD.

A complementary method allowing coverage of the nanometer and sub-nanometer range, consists in counting radiation induced *positive ions*, which undergo a considerably reduced diffusion. First attempts to measure ion signals were undertaken in the early seventies[14, 15, 16, 17], but did not come to practice during that time. A modified approach, which is based on counting ions induced in a gas jet is presently under investigation[18, 19].

Independently, a novel ion counting nanodosimetric technique was recently proposed in our works[20, 21]. The first results presented in this article demonstrate the feasibility of studying ionization effects on the tissue-equivalent DNA scale.

2 The ion counting nanodosimeter

2.1 General concept

The concept of the ion counting nanodosimeter is shown in Figure 1. An energetic charged particle traversing a low-pressure gas ionization cell, typically at about 1 $Torr$, induces ionizations around its track. Radiation-induced ions drift under an electric field E_1, through a narrow aperture, towards an ion counter (under E_2). The electric field configuration and the size of the aperture define the sensitive volume, shown in the figure. In the ion counter, which is a vacuum-operated electron multiplier, fast signals result from multiplied secondary electrons originating from the interaction of vacuum-accelerated ions with the multiplier surface. An appropriate differential pumping system has to maintain the pressure difference between the ionization cell and the ion counter region. Due to the low transverse diffusion of the ions (compared to that of electrons) and their low initial energy, there are practically no lower limits on size of the sensitive volume; sub-nanometer resolution can be reached. Moreover, as charges do not undergo gas multiplication, there are no limits to the type of gas to be investigated. This is a considerable advantage, which permits selection of various gases for simulating the chemical composition of different fine subsystems of the living cell.

2.2 The sensitive volume evaluation

The size and the shape of the sensitive volume depend on the transverse diffusion of the ions during their drift towards the aperture. In addition, the length of the volume along the electric field can be selected by defining the time interval during which arriving ions are detected. Using the known diffusion model[22] one can easily get an expression for average arrival time $\bar{t}$ and rms transverse displacement of an ion, $\bar{x}_{ion}$, during its drift under an electric field,

$$\bar{t} = L/EK \tag{1}$$

$$\bar{x}_{ion} = \sqrt{D/K}\sqrt{2L/E} \quad (2)$$

Here D is the transverse diffusion coefficient , K – the ion mobility, L – the drift distance and E – the electric field strength.

It should be noted that in multiatomic gases (of interest for dosimetry), a multitude of ion species can be produced, each having a different diffusion coefficient and mobility. Moreover, various ion-molecule reactions are possible, which leads to subsequent transformations of the ions during the diffusion process. Therefore, the ion transport data required for the nanodosimeter sensitive volume evaluation should be averaged over the spectrum of the initially produced ion species and over various "transport channels", connected to various transformations during the diffusion. Such data are not available in the literature.

In order to model the expected performance of an ion counting nanodosimeter, a method for measuring ion transport parameters, namely, D/K and K as a function of E/p (p being the gas pressure) has been developed and utilized [21]. These measurements provided distribution functions of the drift time and the transverse diffusion, averaged over all ion species, which are induced by radiation in a given gas and drift in that gas under an applied electric field. The measured data and their analytical approximations for propane, used in this work, are shown in Figure 2. The reduced ion mobility K_0 in Figure 2b is related to K by the equation

$$K_0 = \frac{p}{760}\frac{273}{T}K, \quad (3)$$

where p is the gas pressure in $Torr$ and T is the gas temperature in ($^\circ K$). The average arrival time was calculated using equation (1); according to our measurements, its distributions were approximated as Gaussians, with relative rms deviation of 0.18.

To obtain the sensitive volume size and configuration, a function $f(L, R, t_1, t_2)$ was calculated, which is the probability that an ion, induced in a point (L, R) of the ionization cell, passes through the aperture and reaches the ion detector within the time window (t_1, t_2). The coordinates L and R are the distances from the aperture plane and the aperture axis respectively; t_1 and t_2 are measured from the reference detector pulse (see Figure 1). $f(L, R, t_1, t_2)$ was assumed to be a product $f_1(L, R)f_2(t_1, t_2)$ of two independent probability functions, depending on the ionization point position and on the drift time, respectively. To obtain $f_1(L, R)$, according to the diffusion model[22], a distribution function $\varphi_{L,R}(r)$ was calculated, which represents a probability density for an ion induced in the point (L, R) to reach the aperture plane at a distance r from the aperture center; then $f_1(L, R)$ was calculated as an integral of $\varphi_{L,R}(r)$ taken over the aperture area. The function $f_2(t_1, t_2)$ was calculated as an integral of the drift time distribution over the selected time window. To calculate the sensitive volume without any time selection, $f_2(t_1, t_2)$ is taken to be 1. The calculated sensitive volume configurations for the conditions of our measurements are presented later (see Figures 5 and 6).

2.3 The prototype nanodosimeter setup

A schematic view of the ion counting nanodosimeter prototype setup is shown in Figure 3. It contains three chambers: an ionization cell, a vacuum decoupler and a high vacuum chamber with an ion detector.

The ionization cell is flushed with a low pressure gas. It contains a collimated ^{241}Am α-particle source and a PIN diode (Hamamatsu Photonics S1223-01), providing a reference

signal for the acquisition system. Gas ionization occurs across the ionization cell, by direct α-particle impact, or through the mediation of δ-rays. Under the applied electric field, the ions drift towards a circular aperture; some of the ions (according to the sensitive volume configuration) pass through the aperture and are accelerated towards the ion detector. The reference signal from the PIN diode provides the acquisition system with a trigger induced by the collimated α-particles traversing the whole length of the "region of primary ionization" (see Figure 3b). This is a cylindrical region of 3 mm in diameter and a distance of 4 mm between its axis and the aperture plane. The trigger rate of the α-beam is about 400 particles per second; the aperture diameter is 0.85 mm.

The vacuum decoupler serves to provide a two-stage differential pumping, to maintain the pressure difference between the ionization cell and a high vacuum ion detector region. It contains ion guiding electrodes, which also limit the gas flow into the high vacuum chamber.

The high vacuum chamber is maintained under pressure of the order of 10^{-5} $Torr$, which permits safe operation of the electron multiplier (EM) of a multiple dynode type (*ETP electron multipliers*, Massachusetts, USA; model DM205). The chamber contains electrodes accelerating the ions up to about 3 keV and focusing them into the EM. At this ion energy the EM efficiency was measured to be above 90%. It provides 10 ns wide pulses, far above noise (see Figure 4a).

The acquisition system is based on a Tektronix 2440 digital oscilloscope connected to a PC computer, which is supplied with a program for the signal analysis[23]. The system is triggered by the reference pulse from the PIN diode. An example of an ionization event recorded by the digital oscilloscope is shown in Figure 4a. Identification of the individual ion-induced pulses is made by a signal analysis program using a correlation method[24]. Each recorded event corresponds to a sequence (cluster) consisting of one or several ions induced within the sensitive volume (in a direct or an indirect way) by a single α-particle detected with the PIN diode. Frequency distributions of the ion cluster sizes, i. e., the number of ions in a cluster, are obtained from a series of records. An additional selection of the sensitive volume size, in the direction parallel to the electric field, is made by counting ions within a selected time window, as shown in Figure 4b.

3 Results and discussion

3.1 The sensitive volume

One of the important practical aspects of an ion counting nanodosimeter is the ability to form a sensitive volume of a desirable tissue-equivalent size. As discussed above, the sensitive volume size and configuration in the laboratory frame depend on the aperture geometry, the applied electric field strength, and the ion transport parameters; the scaling factor connecting the laboratory frame size with the tissue-equivalent one is proportional to the gas density. While there is practically no lower limit to the sensitive volume size, its upper limit depends on the highest possible gas pressure in the ionization cell. The latter, in turn, is limited by the design and the efficiency of the differential pumping system; it should provide an acceptable vacuum in the region of the electron multiplier. A two stage differential pumping system in the present setup permits reaching a propane pressure of about 0.75 $Torr$, maintaining the vacuum at the EM on the level of 10^{-4} $Torr$; this is the upper permissible vacuum limit for its operation. Improving the differential pumping system should permit a pressure

increase by a factor of 2 or 3, and, therefore, corresponding increase of the sensitive volume dimensions.

Calculated configurations of the sensitive volume for propane at 0.54 and 0.73 $Torr$ are presented in Figure 5. They are shown as contour plots of the efficiencies of extracting ions, originally induced by radiation in various locations of the ionization cell. The contour plots are presented for two very different extraction electric field strengths, further discussed below. One can see that, in both cases, the sensitive volumes (within the efficiency contour of 0.5) form approximately cylindrical regions, with a diameter corresponding to that of the aperture (0.85 mm). Its length-to-diameter ratio strongly depends on the electric field strength, and varies from a value of 3 under the low electric field condition of 16.8 V/cm (Figure 5a) to a value of 8 under the high field condition of 210 V/cm (Figure 5b). The corresponding sensitive volume tissue-equivalent sizes (diameter×length) are 1.1 $nm \times 3$ nm and 1.5 $nm \times 12$ nm, respectively. To achieve smaller, more precise defined sensitive volumes, the extended sensitive volume formed under the high extracting field can be further divided by applying time selection windows. This way, completely closed wall-less sensitive volumes can be formed (Figure 6).

According to our recent model estimations, the most biologically relevant sensitive volume is a cylinder of about 2 nm in diameter and 8 to 16 nm in length. Such volume has been practically reached with our technique. Further increase of the tissue-equivalent sensitive volume is possible by increasing the gas pressure (which requires improving the pumping system), or by increasing the gas pressure in combination with reducing the aperture diameter (maintaining the same gas flow), as discussed in our previous work[21].

3.2 Ion cluster distributions

The measurements of the ion cluster distributions were performed under two different electric field strengths.

Low extraction field. An example of an ion cluster distribution spectrum, obtained in 0.54 $Torr$ propane under an electric field of 16.8 V/cm, is shown in Figure 7. One can see that clustered ionization events were detected, reaching a value of 9 ions per cluster at the 10^{-4} level. The electric field was defined by a 8.4 V potential difference across the 5 mm spaced electrodes (Figure 3). This voltage was chosen below the gas ionization potential to prevent additional ionizations by slow secondary electrons accelerated within the ionization cell. Therefore, the observed ion clusters are those induced by single α-particles (directly or via the δ-rays). The obtained distribution can be considered as a true nanodosimetric spectrum, measured in a given tissue-equivalent sensitive volume. From Figure 5a, one can see that the total volume size (without any time selection) is about 1.1 $nm \times 3$ nm. However, the data spectrum in Figure 7 was obtained with a time selection window of 4 μs, which, according to the measured ion transport parameters, corresponds to an ion drift distance of 0.75 mm, or to approximately 1 nm on a tissue-equivalent scale. Therefore, the spectrum in Figure 7 corresponds to a tissue-equivalent sensitive volume of 1.1 nm in diameter and 1 nm in length.

High extraction field. As discussed above, biologically relevant sensitive volumes require high extracting electric field conditions. However, in the present version of our instrument,

the high applied electric field induces some charge multiplication, which leads to significant distortion of the initially deposited ion distribution.This phenomenon occurs, because the electrons ejected in radiation-induced ionization processes are accelerated under the electric field and may gain sufficient energy to cause further ionizations. The electron multiplication is generating an excessive number of ions within the sensitive volume, and therefore the obtained ion cluster spectra do not represent true nanodosimetric spectra. Nevertheless, the sensitive volume size and configuration do not depend on the charge multiplication processes and remain unchanged; the resulting ion cluster distribution spectra represent the cluster distribution of the total number of deposited ions in this volume, regardless of their mechanism of deposition. This permits preliminary testing the apparatus with large sensitive volumes formed under the high electric field conditions.

Examples of spectra obtained under these conditions (210 V/cm, 0.73 $Torr$) are shown in Figure 8. All histograms in this figure were obtained from the same set of recorded pulse sequences by counting the number of pulses within various time intervals, corresponding to the sensitive volume configurations shown in Figures 6. The histogram a shows a relatively small average number of ions in a cluster, as the core of the corresponding sensitive volume is outside the primary ionization region (Figure 3); here the radiation induced ions are formed mostly by the δ-rays emitted across the particle track; the secondary electrons emitted in other parts of the ionization cell do not contribute to ion formation, as they are accelerated in the opposite direction. The ion yield and the average number of ions in a cluster are significantly larger in histograms b and c. Histogram c, measured in the largest sensitive volume, exhibits the highest values of ion yield and the largest ion clusters.

The high electric field conditions results demonstrate the ability to obtain nanodosimetric spectra from sensitive volumes, the dimensions of which can be selected off-line, while processing the stored data. However, in order to have data which are valuable for nanodosimetry, the distortion of the ion distributions caused by charge multiplication should be eliminated. This can be achieved by the following technique: the high stationary electric field is substituted by a pulsed field, applied with a certain delay after the passage of the primary ionizing particle. During this delay, within a few tens of nanoseconds all radiation-deposited electrons will be cleared out of the sensitive volume under a low electric field. Upon application of the high electric field pulse, only the radiation-induced ions will be present in the ionization cell; they practically can not cause further ionization during their extraction, and the real distribution of the radiation-induced ions will not be distorted.

4 Conclusions

The results presented in this work are a first demonstration of the ability to obtain nanodosimetric spectra on a scale of the DNA, by a novel single ion counting method. This method permits definition of a small wall-less sensitive volume, well distanced from any solid material in the device. Off-line time distribution analysis of a single collected data set provides nanodosimetric spectra corresponding to various sizes and locations of the sensitive volume.

The reported technique is able to provide nanodosimetric data for sites in the range from a fraction of a nanometer up to a few nanometers in diameter and few tens of nanometers in length. Thus, it covers the DNA-relevant range of sizes. Combined with other modern nanodosimetric and microdosimetric methods, it will permit to cover the whole range of relevant cellular target sizes.

The new technique is not limited to biological samples. It provides ways of studying radiation damage to sub-micrometric electronic devices, a field of prime importance in particle physics and space science.

Acknowledgments

The authors would like to thank G. Garty for assistance with the data acquisition, and M. Klin for technical assistance. This work was partly supported by a US National Medical Technology Testbed grant (No. DAMID 17-97-2-7016), the Foundation Mordoh Mijan de Salonique the Israel Science foundation, and a European Commission grant (No. FI4P-CT96-0044). S. S. is partly supported by the Israel Ministry of Immigration. A. B. is the W. P. Reuther Professor of Research in the peaceful uses of Atomic Energy. R. W. M. S. would like to thank Dr. J. M. Slater for his continued interest and support at Loma Linda University Medical Center.

References

1. Ward J.F. *The complexity of DNA damage - relevance to biological consequences.* Int. J. Rad. Biol. 66, 427-432, (1994).

2. Goodhead D.T. Initial events in the cellular effects of ionizing radiations: clustered damage in DNA. Int. J. Radiat. Biol. 65, 7-17, (1994).

3. Prise K.M., Folkard M., Newman H.C., and B.D. Michael. *Effect of radiation quality on lesion complexity in cellular DNA.* Int. J. Rad. Biol. 66, 537-542, 1994.

4. Goodhead D., O'Niell P., Menzel H. (ed.) *Microdosimetry: An Interdisciplinary Approach.* the Royal Society of Chemistry (Cambridge), preface to the book. ISBN 0-85404-737-9 (1997).

5. Goodhead D. T. *Relationship of Microdosimetric Techniques to Applications in Biological Systems.* In: The Dosimetry of Ionizing Radiation, v. 2, ed. Kase K. R, Bjärngard B. E. B., Attix F. H., Academic Press, 1-89 (1987).

6. Schulte R. W. M. *Prediction of Cellular Effects of High- and Low-LET Irradiation Based on the Energy Deposition Pattern at the Nanometer Level.* In: Microdosimetry: An Interdisciplinary Approach, ed. Goodhead D., O'Niell P., Menzel H., the Royal Society of Chemistry (Cambridge), 211-214. ISBN 0-85404-737-9 (1997).

7. Colautti, P., Cutaia M., Makarewicz M., Schraube H., Talpo G., Tornielli G.*Neutron microdosimetry in simulated volumes less than 1 μm in diameter.* Radiat. Prot. Dosim. 13, no. 1-4, 117-121 (1985).

8. Kliauga P. *Measurement of single event energy deposition spectra at 5 nm to 250 nm simulated site sizes.* Radiat. Prot. Dosim. 31 , no. 1-4, 119-123 (1990).

9. Anachkova E., Kellerer A.M., Roos, H. *Neutron energy deposition spectra at simulated diameters down to 50 nm.* Radiat. Prot. Dosim. 70, no. 1-4, 207-210 (1997).

10. Pansky A., Malamud G., Breskin A. and Chechik R. *Application of gaseous electron counting detectors.* Nucl. Instrum. and Meth. A 323, 294-308 (1992).

11. Colautti P., Talpo G., Tornielli G., Akkerman A. and Breskin A. *Measurements of ionization distribution around a particle track at the nanometer level.* Radiat. Prot. Dosim. 52, 329-334 (1994).

12. Breskin A., Chechik R., Colautti P., Conte V., Pansky A., Shchemelinin S., Talpo G. and Tornielli G. *A single-electron counter for nanodosimetry.* Radiat. Prot. Dosim. 61, 199-204 (1995).

13. Titt U., Breskin A., Chechik, R., Dangendorf V., Schmidt-Böcking H., Schuhmacher H. *A time projection chamber with optical readout for charged particle track structure imaging.* Submitted to Nucl. Instrum. and Meth. (1998)

14. Pszona S., COO 3243-2 Report, USAEC, New York, (1973).

15. Chmelewski D., Parmentier N. and Le Grand J., EUR 5122 d-e-f Report, 969, (1974).

16. Pszona S., EUR 3452 d-e-f Report, 1107, (1975).

17. Pszona S. *A track ion counter.* Proc. Symp. Microdosim., 5th, Verbania Pallanza, Italy, 1975, 1107-1121. Comm. Eur. Communities [Rep.] EUR-5452.

18. Pszona S. and Gajewski R. *An Approach to Experimental Microdosimetry at the Nanometre Scale.* Radiat. Prot. Dosim. 31, no. 1-4, 427-430 (1994).

19. Pszona S. *Ionization measurements in nanometer size sites with jet counter - recent experimental results.* In: Microdosimetry: An Interdisciplinary Approach, ed. Goodhead D., O'Niell P., Menzel H., the Royal Society of Chemistry (Cambridge), 395-398. ISBN 0-85404-737-9 (1997).

20. Shchemelinin S., Breskin A., Chechik R., Pansky A., Colautti P., Conte V., De Nardo L. and Tornielli G. *Ionization measurements in small gas samples by single ion counting.* Nucl. Instrum. and Meth. A 368, 859-861 (1996).

21. Shchemelinin S., Breskin A., Chechik R., Pansky A., Colautti P. A nanodosimeter based on single ion counting. In: Microdosimetry: An Interdisciplinary Approach, ed. Goodhead D., O'Niell P., Menzel H., the Royal Society of Chemistry (Cambridge), 375-378. ISBN 0-85404-737-9 (1997).

22. McDaniel E. W., Mason E. A, *Transport Properties of Ions in Gases.* Wiley, New York, ISBN 0-471-88385-9 (1987).

23. Malamud G., Breskin A. and Chechik R. *A systematic study of Primary Ionization Cluster Counting at Low Gas Pressure.* Nucl. Instrum. and Meth. A 307, 83-96 (1991).

24. Black W. W. *Application of Correlation Techniques to Isolate Structure in Experimental Data.* Nucl. Instrum. and Meth. 71, 317-327 (1969).

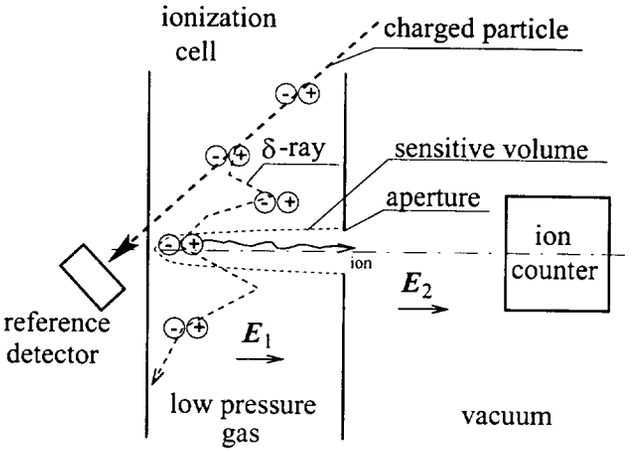

Figure 1
A conceptual diagram of the single ion counting method. Ions, released by a charged particle within the sensitive volume of a low-pressure gas ionization cell, drift through an aperture and, following acceleration, are counted in a vacuum-operated device.

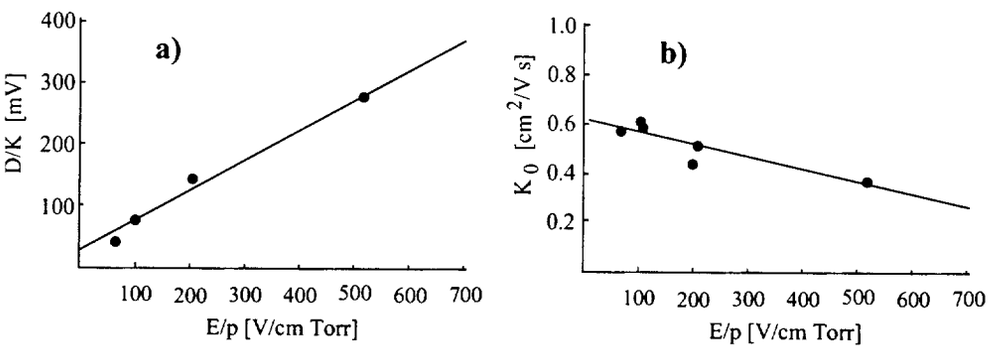

Figure 2
Measured (points) and analytically approximated (lines) ion transport parameters.
a) Transverse diffusion to mobility ratio and its approximation $D/K = 27 + 0.491\ E/p$. The D/K value at E/p=0 is taken according to the Einstein relation[22].
b) Reduced mobility and its approximation $K_0 = 0.618 - 0.000498\ E/p$.

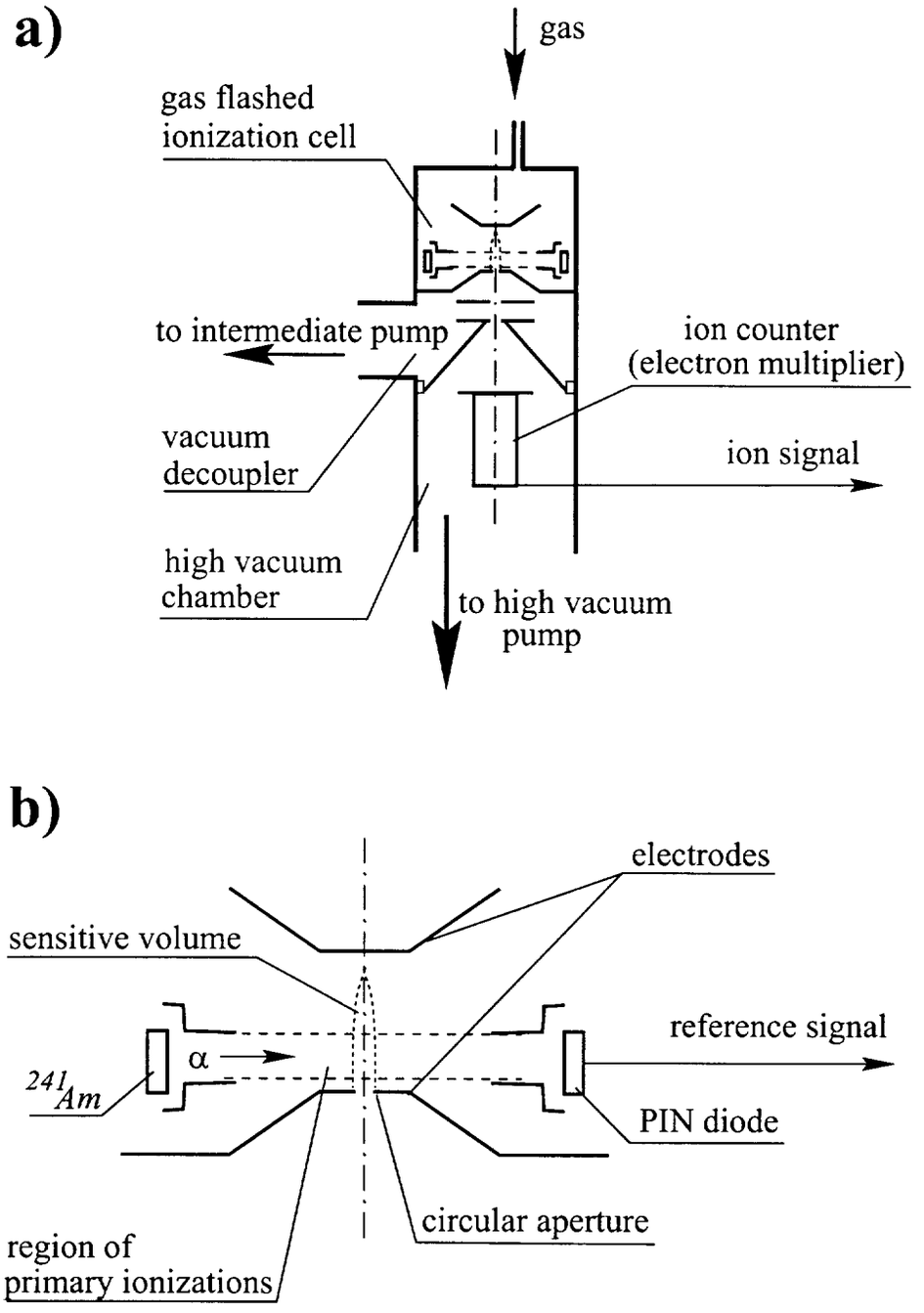

Figure 3
The laboratory ion counting prototype.
a) General schematic view.
b) An enlarged view of the ionization cell. The distance between the electrodes is 5 and 10 *mm* in the low and high field measurements, respectively.

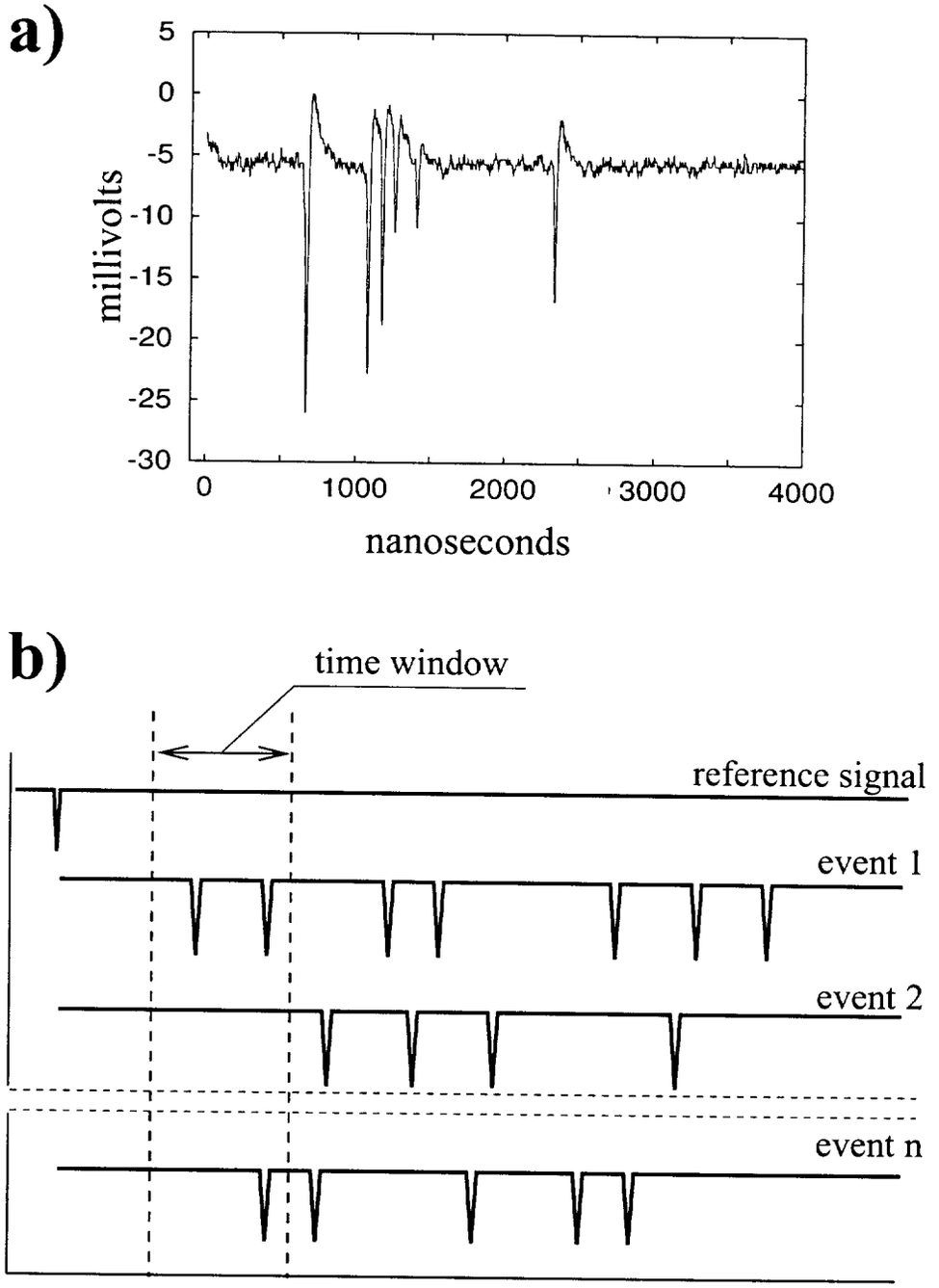

Figure 4

a) An example of a recorded ionization event with a six ion cluster; propane, 0.65 $Torr$, E=210V/cm. The pulse sequence from the ion detector, after a fast preamplifier, was recorded using a Tektronix 2440 digital oscilloscope (4 ns digitization bins).

b) A schematic representation of the off-line longitudinal selection of the sensitive volume. The signal analysis program counts the number of pulses only within the time window. Different event records are shown.

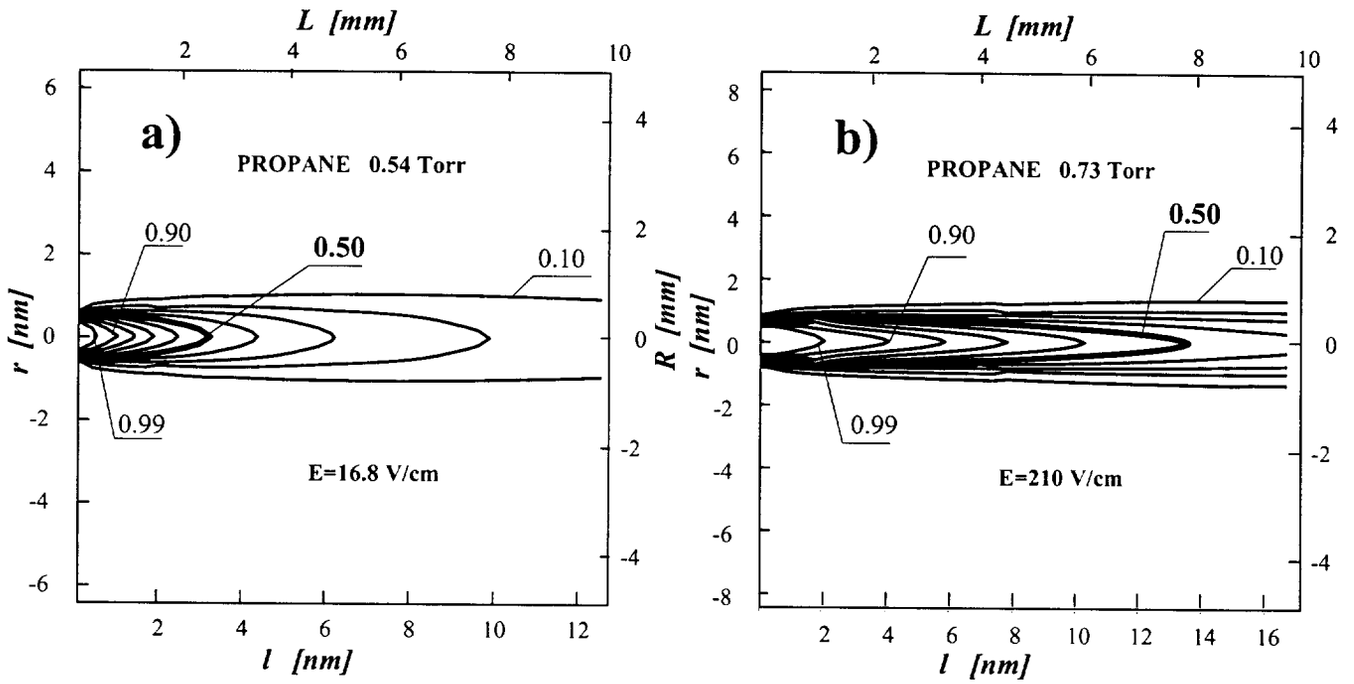

Figure 5
Calculated sensitive volume configurations at two gas pressures and very different electric field strengths, without arrival time selection; the aperture diameter is 0.85 mm. The contour plots represent the collection efficiency of ions deposited in a point (L, R) of the ionization cell. L and R are the laboratory scale distances (in millimeters) from the aperture plane and the aperture axis correspondingly; l and r are the corresponding distances (in nanometers) on the tissue-equivalent scale.

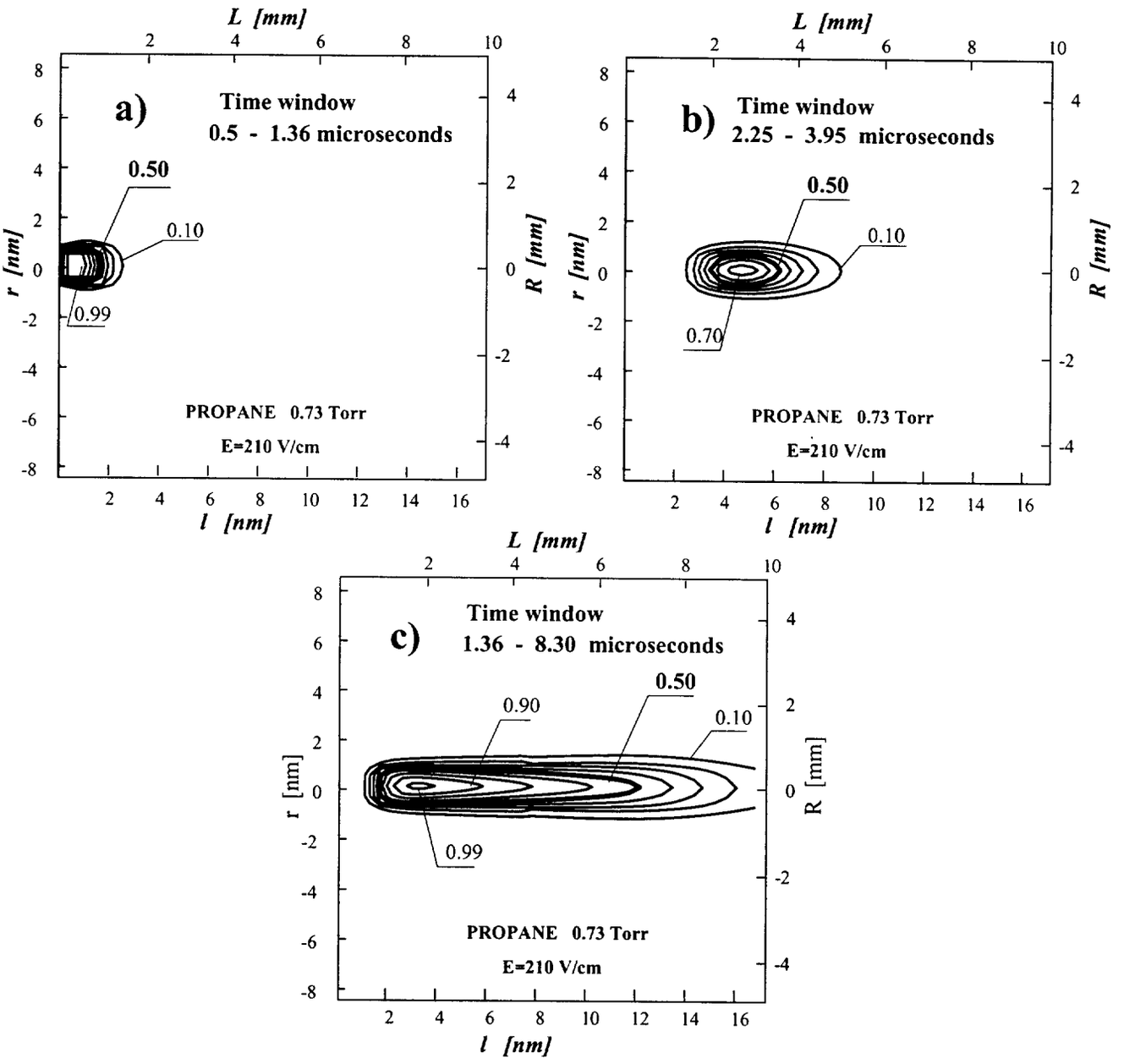

Figure 6
Partial sensitive volumes selected from an initially larger volume (Figure 5b) using time windows, as shown in Figure 4b. The plot coordinates and the contour levels are the same as in Figure 5. The time windows are indicated in the plots.

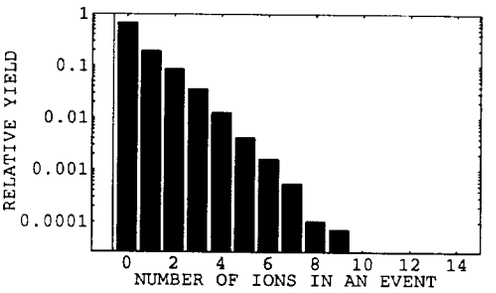

Figure 7
A measured nanodosimetric spectrum of ion clusters deposited by α-particles in a propane tissue-equivalent volume of 1.1 $nm \times 1nm$ (diameter×length). The histogram is normalized to the number of detected α-particles.

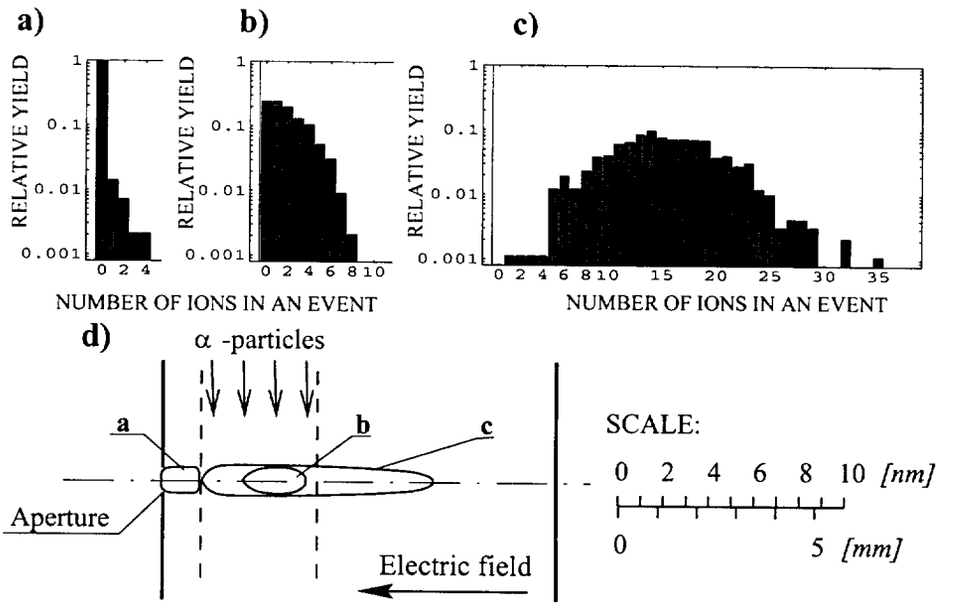

Figure 8
Measured nanodosimetric spectra of ion clusters, deposited in time selected tissue-equivalent propane volumes, of various sizes and locations along the ion drift axis. The spectra a, b and c correspond to the sensitive volumes marked in d. The same volume configurations are shown in Figure 6 in more details. All spectra in this figure was obtained from the same data set by off-line processing. The distributions comprise both radiation-induced ions and additional avalanche-induced ions under the high applied electric field of 210 V/cm (see text for discussion)